

Simulations of spectral lines from an eccentric precessing accretion disc

Stephen B. Foulkes¹, Carole A. Haswell¹, James R. Murray^{2,3}, Daniel J. Rolfe^{1,2}

¹*Department of Physics & Astronomy, The Open University, Walton Hall, Milton Keynes, MK7 6AA, UK.*

²*Department of Physics & Astronomy, University of Leicester, University Road, Leicester, LE1 7RH, UK.*

³*Department of Astrophysics & Supercomputing, Swinburne University of Technology, Hawthorn, VIC 3122, Australia.*

Email SBF: sbfoulkes@qinetiq.com, CAH: C.A.Haswell@open.ac.uk, JRM: jmmurray@astro.swin.edu.au, DJR: dj@astro.le.ac.uk

Accepted. Received

ABSTRACT

Two dimensional SPH simulations of a precessing accretion disc in a $q = 0.1$ binary system (such as XTE J1118+480) reveal complex and continuously varying shape, kinematics, and dissipation. The stream-disc impact region and disc spiral density waves are prominent sources of energy dissipation. The dissipated energy is modulated on the period $P_{sh} = (P_{orb}^{-1} - P_{prec}^{-1})^{-1}$ with which the orientation of the disc relative to the mass donor repeats. This superhump modulation in dissipation energy has a variation in amplitude of $\sim 10\%$ relative to the total dissipation energy and evolves, repeating exactly only after a full disc precession cycle. A sharp component in the light curve is associated with centrifugally expelled material falling back and impacting the disc. Synthetic trailed spectrograms reveal two distinct ‘S-wave’ features, produced respectively by the stream gas and the disc gas at the stream-disc impact shock. These S-waves are non-sinusoidal, and evolve with disc precession phase. We identify the spiral density wave emission in the trailed spectrogram. Instantaneous Doppler maps show how the stream impact moves in velocity space during an orbit. In our maximum entropy Doppler tomogram the stream impact region emission is distorted, and the spiral density wave emission is suppressed. A significant radial velocity modulation of the whole line profile occurs on the disc precession period. We compare our SPH simulation with a simple 3D model: the former is appropriate for comparison with emission lines while the latter is preferable for skewed absorption lines from precessing discs.

Key words: accretion: accretion discs - X-rays: binaries - binaries: low mass X-ray binaries, cataclysmic variables - stars: individual: A 0620-00, XTE J1118+480, GRO J1655-40 - methods: numerical

1 INTRODUCTION

Superhumps are photometric modulations in the observed light curves found in some short period cataclysmic variables (CVs) (Patterson 1998), and in some of the transient low mass X-ray binaries known as soft X-ray transients (SXTs) (Zurita et al. 2002). In general the superhump period, P_{sh} , is a few percent longer than the binary orbital period, P_{orb} , and is attributed to the prograde apsidal precession of a non-axisymmetric accretion disc. Such precession is expected in extreme mass ratio systems ($q \lesssim 0.3$, where $q = M_2/M_1$ is the mass ratio) in which the disc encompasses the 3:1 resonance (Lubow 1991). If the disc extends to the 3:1 resonant radius, it becomes eccentric and non-axisymmetric (Murray 1998) and it will then precess under the tidal influence of the secondary star. In CVs, superhumps in the light curve are understood as being powered directly from the

modulated tidal stresses (Osaki 1985; Murray 1998). This modulation is accompanied by a change in the solid angle subtended by the disc at the central X-ray source, and it is this shape change which leads to the irradiation-powered superhumps in X-ray bright SXTs (Haswell et al. 2001).

Material from the donor star leaves the first Lagrangian point (L_1) and flows along a ballistic trajectory towards the central primary object. When this gas stream encounters the accretion disc material, large amounts of energy are dissipated in a brightspot region on the outer edge of the disc. As the eccentric accretion disc precesses in the inertial frame, and the orbital motion of the binary proceeds, the energy dissipated at the brightspot will be modulated as described by Rolfe, Haswell & Patterson (2001 hereafter RHP2001).

Spectroscopic observations of superhumping CVs (Vogt 1982; Hessman et al. 1992; Patterson et al. 1993a)

and SXTs (in particular XTE J1118+480) have shown that trailed spectrograms of such objects are complex and change from night to night (Torres et al. 2002; Zurita et al. 2002; Haswell et al. 2004). Over intervals of days or months (many times the orbital period) the spectral line profiles evolve from almost symmetric to enhanced red-shifted or blue-shifted. These changes have been attributed to a precessing accretion disc, and herein we present calculations which strongly support this interpretation.

In this paper we describe the results from two simulations of a precessing eccentric accretion disc. The first simulation consisted of a simple analytical three-dimensional representation of the disc and brightspot region based on RHP2001. The second model was a high-resolution smoothed particle hydrodynamics (SPH) simulation. SPH is a Lagrangian numerical method for modelling fluid flow using a set of moving particles. The fluid properties at any point within the flow field are determined by interpolating from the local particle properties. This interpolation takes the form of a summation over the local particles, weighted according to their distance from the evaluation point. For a comprehensive review of the method see Monaghan (1992).

In section 2 we detail the binary system modelled and the two numerical methods employed to model the system. Section 3 presents our results and Section 4 is devoted to discussion and conclusions.

2 SIMULATIONS

2.1 Binary Parameters

To simulate a typical SXT, we adopted a mass ratio $q = 0.1$. The orbital period, P_{orb} , is $(4\pi^2 a^3 / GM_t)^{1/2}$, where a is the orbital separation, and M_t is the total mass of the binary system. The mass transfer rate was $1.46 \times 10^{-9} M_t \text{yr}^{-1}$.

2.2 Simple Analytical Approximation to a Precessing Eccentric Disc

Here we briefly describe a simple model for the eccentric disc and stream-disc impact developed from that used to model late superhumps in the SU UMa CV IY Uma, see RHP2001. The model assumes the brightspot emission is directly proportional to the kinetic energy of the relative motion of the stream and disc flows at the impact point, i.e. the rate of energy dissipation at the brightspot is:

$$\dot{E} = \frac{1}{2} \dot{M} V_{rel\perp}^2 + \frac{1}{2} \dot{M} V_{rel\parallel}^2 \frac{V_{rel\parallel}}{|V_{rel\parallel}|}$$

where \dot{M} is the mass flow rate of the stream and $V_{rel\perp}$ and $V_{rel\parallel}$ are the relative velocity of the stream and disc resolved perpendicular and parallel to the disc respectively. The disc velocity at radius r from the primary object is assumed to be that of an elliptical orbit around the primary object, that is:

$$|\vec{V}_{disc}| = \sqrt{GM_1 \left(\frac{2}{r} - \frac{1}{a_{orbit}} \right)},$$

where a_{orbit} is the semi-major axis of the orbit and M_1 is the mass of the primary object. The velocity of the stream \vec{V}_{stream} is simply that of the ballistic trajectory.

The model includes a simple 3D structure for the brightspot region. An elliptical cross-section in the r-z plane is assumed, with size r_{spot} and h_{spot} ¹ centred on the outer disc edge. r_{spot} , h_{spot} and the spot brightness decrease downstream from the initial impact as $e^{-\theta^2 / \Delta\theta_{spot}^2}$ where θ is the angular distance downstream from the initial impact point. Upstream of the impact the brightspot surface is rounded off with a hemisphere of uniform brightness equal to that at the initial impact. We used $r_{spot} = 0.03a$ and $h_{spot} = 0.012a$ at $\theta = 0$ (a is the binary separation). The angular extent of the brightspot region is set by $\Delta\theta_{spot} = \Delta\theta_0 a_{disc} / r_0$, where r_0 is the disc radius at the impact point and a_{disc} is the semi-major axis of the disc. This keeps the arc length of the brightspot region roughly constant at $\Delta\theta_0 a_{disc}$ as the eccentric disc precesses. We used $\Delta\theta_0 = 30^\circ$.

The disc was modelled as an ellipse with $a_{disc} = 0.31a$ and eccentricity 0.093 at the outer edge². Streamlines and brightness contours within the disc are ellipses with size and eccentricity decreasing smoothly to zero at the primary object, with the velocity given by $|\vec{V}_{disc}|$. The inner boundary is near-circular with radius $0.025a$. The disc brightness varies as $a_{orbit}^{-1.2}$. The disc is flared with total thickness increasing linearly from 0 at the primary object to $0.02a$ at the outer edge. An orbital inclination of 70° was used to avoid eclipses.

In the brightspot region, where the stream and disc flows merge, we adopted a velocity distribution which was non-zero between the local disc velocity at that point, \vec{V}_{disc} , and the velocity $\vec{V}_{disc} + (\vec{V}_{stream,0} - \vec{V}_{disc}) e^{-\theta^2 / \Delta\theta_{spot,v}^2}$. Thus, at the impact point, velocities between \vec{V}_{disc} and the ballistic stream velocity at the impact, $\vec{V}_{stream,0}$ contribute to the Doppler broadening of the local line profile. Downstream the local velocity smoothly approaches the disc velocity. Upstream of the impact the exponential factor was set to 1. $\Delta\theta_{spot,v}$ behaves as $\Delta\theta_{spot}$ as the eccentric disc precesses. We used $\Delta\theta_{0,v} = 5^\circ$.

The local linewidths were assumed to have Gaussian profiles, with the disc width set to the disc thermal velocity. The brightspot profile width was the quadratic sum of the disc thermal velocity and the thermal velocity of a 10^4K source decaying as $e^{-\theta^2 / 4\Delta\theta_{spot}^2}$ downstream. The decay was imposed for consistency with the brightspot brightness, assuming brightspot brightness $\propto T_{brightspot}^4$.

2.3 SPH Simulation

The accretion disc was also modelled using a two-dimensional SPH computer code that has been described in detail in Murray (1996, 1998). Modifications have been made to convert the code from FORTRAN to C++. C++ is an Object Orientated computer language allowing each particle to have its own private attributes (e.g. position, velocity) and particle interactions can be coded in a more flexible manner. The code was also extended to allow its execution on an array of processors using the Message-Passing Interface Standard³. The SPH results presented here were generated on a small private Linux network.

In the SPH simulation the total system mass, M_t , and

¹ See Figure 8 of RHP2001.

² The eccentricity was chose to match that of our SPH simulation

³ <http://www-unix.mcs.anl.gov/mpi/>

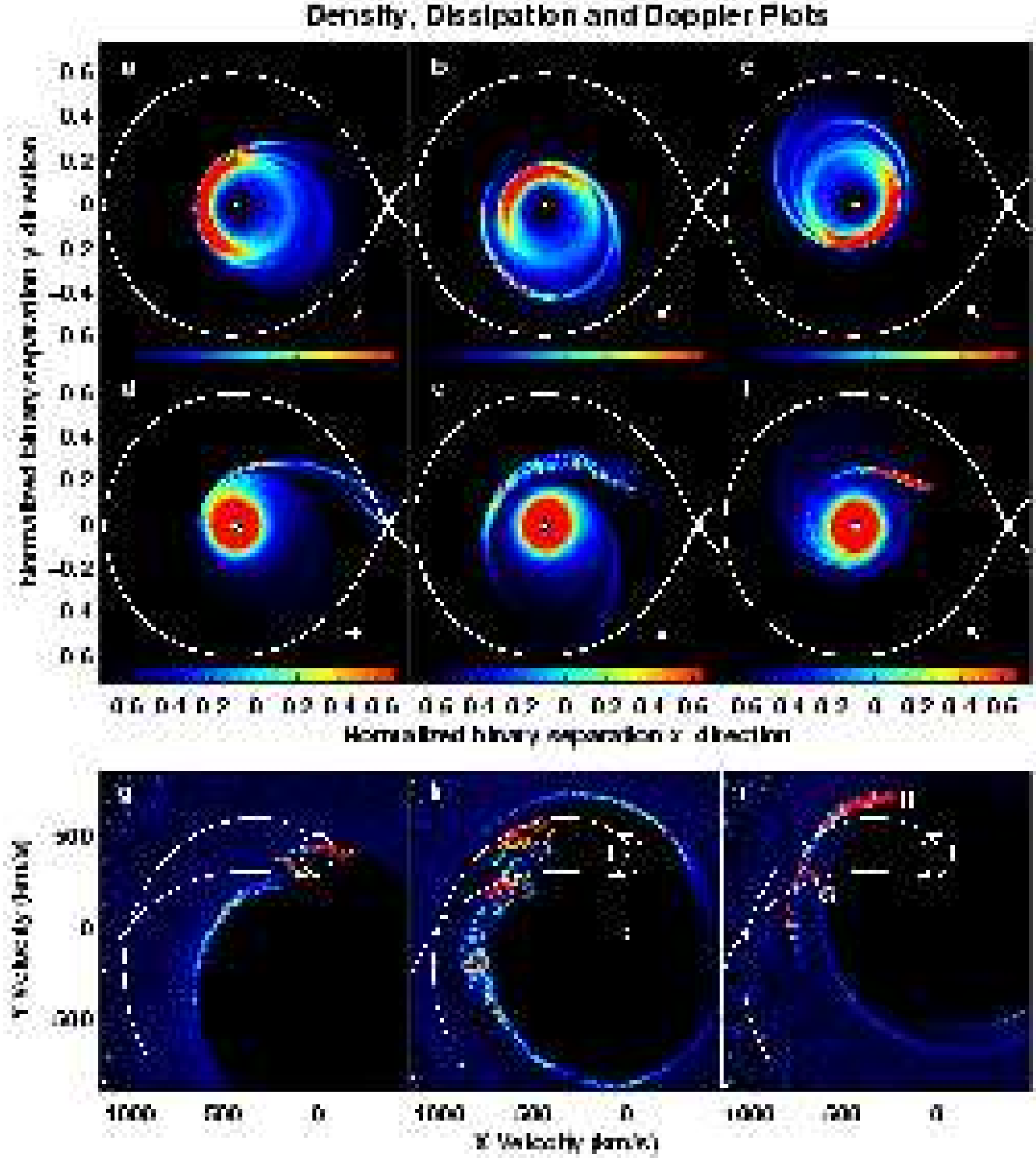


Figure 1. The top row (a, b, c) are accretion disc surface density maps using a logarithmic colourscale for binary phases 0.00, 0.36, and 0.64 respectively. The secondary orbits anti-clockwise with respect to the inertial frame, with mass being added from the L_1 point at the right of each map. The solid curve is the Roche lobe of the primary, plotted in a frame that co-rotates with the binary. The arrow in the lower right-hand corner of each map indicates a fixed direction to an observer. The middle row (d, e, f) are the corresponding dissipation maps plotted with a logarithmic colourscale. The bottom row (g, h, i) are the matching Doppler maps plotted using a linear colourscale. The letter “G” on map i, indicates the point at which the gas stream impacts on the outer edge of the accretion disc and the letter “H” indicates the arc of emission produced by the disc particles in the impact region.

the binary separation, a , were both scaled to unity. The binary orbital period, P_{orb} , was scaled to 2π . The accretion disc had an open inner boundary condition in the form of a hole of radius $r_1 = 0.025a$ centred on the position of the primary object. Particles entering the hole were removed from the simulation. Particles that re-entered the secondary Roche lobe were also removed from the simulation as were particles that were ejected from the disc and had a distance $> 0.9a$ from the centre of mass of the primary.

The artificial viscosity term of Murray (1996) was used to improve the effective shear viscosity in the SPH equations of motion. In the inner regions ($< \sim 0.12a$) of the accretion disc the particles generally executed circular orbits, and the radial shear term dominated the inner disc dissipation. However, in the outer disc the tidal interaction of the secondary was stronger and the bulk term was more significant. The disc energy dissipation was calculated using the SPH energy equation as in Murray (1996). The Shakura-Sunyaev (1973) viscosity parameters were set to α_{low} of 0.1 and α_{high} of 1.0, and the viscosity switched from low to high as described in Truss et al. (2000). The SPH smoothing length, h , was allowed to vary in both space and time and had a maximum value of $0.01a$.

The SPH code was started with no particles, i.e. zero mass in the accretion disc. A single particle was injected into the simulation every $0.01\Omega_{orb}^{-1}$ at the first Lagrangian point. The sound speed in the donor atmosphere was used as the initial speed of each particle and they followed a ballistic trajectory. Within twenty binary orbits the resulting disc became eccentric and encountered the Lindblad 3:1 resonance. After the disc had reached a mass equilibrium state, we followed its evolution through four disc precession cycles (~ 180 binary orbits) to produce the results described here. There were approximately fifty-three thousand particles in the disc, and the average number of ‘neighbours’, that is the average number of particles used in the SPH update equations, was 8.9 particles.

The complicated hydrodynamics of the stream-disc impact have been investigated analytically by Hessman (1999) and numerically by Armitage & Livio, first with the SPH technique (1996) and later with the grid based ZEUS code (1998). In the latter paper, they found the character of the stream-overflow in particular depended strongly upon the equation of state. Kunze, Speith & Hessman (2001) comprehensively studied the impact with much higher resolution SPH simulations, for a range of binary mass ratios. They showed that a substantial fraction (perhaps more than half) of the stream overflowed the outer disc edge, to impact the disc close to the circularisation radius. The latter paper is particularly relevant as it demonstrates that the detailed shock structure of the impact region can be captured using the SPH technique, if sufficient numbers of particles are deployed. The computational cost is however so great as to make a calculation following the evolution of a disc prohibitively expensive.

As our SPH calculations are two dimensional, stream-overflow cannot occur and the brightness of the hot spot will be overemphasised by a factor determined by cooling in the stream. The SPH results presented in the following section will show that the complex stream-disc interaction region dominates the energy dissipation signature of the accretion disc. In a three dimensional SPH code stream-overflow will

occur and hence the hot spot region will have a reduced contribution to the energy dissipated. However, the hot spot region will still contribute a significant amount to the total dissipation observed from the accretion disc.

3 RESULTS

3.1 Disc morphology: orbital modulation

In this subsection we follow the evolution of the SPH simulated accretion disc through a complete binary orbit. The images (a, b, c) in Figure 1 are a set of surface density maps, plotted in the co-rotating frame, for orbital phases 0.00, 0.36 and 0.64 respectively. Each map uses the same logarithmic colourscale, with blue representing low density and red high, we have also plotted the primary Roche lobe. Since we can view the disc from any angle, we have arbitrarily fixed the conjunction of the primary (and hence zero orbital phase) to correspond to Figure 1(a). The arrow in the lower right-hand corner of each map indicates a fixed direction in the inertial frame and we calculate radial velocities as they would be observed by an observer in this direction.

These density maps show the disc to be asymmetric, eccentric and continuously changing shape under the tidal influence of the donor star; its overall position is moving only very slowly in the inertial frame. There are wrapped spiral density waves that extend from the outermost regions of the disc down to approximately the circularisation radius of the system. These produce shear and dissipation in the outer regions of the disc. The spiral density waves propagate angular momentum outwards, thus allowing the disc gas to move inward towards the central primary object. The precession of the disc means that the density maps do not repeat from one orbit to another; instead the maps repeat on a period a few percent longer than the orbital period.

We have placed a Microsoft AVI movie of the change in surface density as function of orbital phase on an Internet web-site (see <http://physics.open.ac.uk/FHMR/> for more information).

3.2 Light curve

In Figure 1(d, e, f), we have plotted viscous dissipation maps corresponding to the density maps in Figure 1(a, b, c). Each dissipation map is represented using the same logarithmic colourscale with blue low dissipation and red high. It is clear from this set of images that the inner disc is in a state of constant high dissipation. The spiral compression waves and the impact of the gas stream on the outer edge of the disc also generate high levels of dissipation.

We are unable to directly resolve the morphology of the accretion disc in observed interacting binary star systems. The simplest directly observable quantity which reveals some of the underlying properties is the light curve. Hence we use the SPH model to simulate the disc luminosity and generate an artificial light curve. We assume that the luminosity is generated through viscous dissipation which is promptly radiated away from the point at which it was generated. The simulated light curve can be directly compared with the observations. We must, however, bear in mind that in observed systems there will generally be

an orbital modulation in the visibility of each location in the co-rotating frame. Hence, our simulated light curves, in which we have essentially assumed 100% visibility for each location throughout the orbit, are likely to be simpler than observed light curves.

The upper left plot of Figure 2 shows five simulated light curves. The upper curve corresponds to the total viscous dissipation from the whole disc; the lower four curves correspond to the four smaller annuli defined in Figure 2 caption. The dissipation in the inner disc ($\lesssim 0.12a$, intermediate between ‘c’ and ‘d’ in Figure 2) is constant, except for stochastic noise. The lower left-hand plot is the dissipation from the innermost disc region and was generated by subtracting dissipation light curve *b* from dissipation light curve *a*. Subtracting curve *c* from *a* and subtracting curve *c* from *b* would also produce similar constant dissipation curves. Superimposed on this, for disc regions ($r > 0.2a$) there is a repeating series of “humps.” These humps recur on the superhump period, P_{sh} . The modulation consists of two separate components. The first is the relatively smooth continuous modulation, which has a minimum at orbital phase 0.0 in Figure 2 (corresponding to Figure 1(a, d)) and reaches a maximum at orbital phase ~ 0.64 , (corresponding to Figure 1(c, f)). The second is the much sharper spiky signal with a short duration which appears at orbital phase ~ 0.36 and corresponds to Figure 1(b, e). Photometric superhumps are invariably detected in optical light. Since the hot inner regions of a viscously-heated disc contribute relatively little to the total optical light, the comparison between observation and our simulation might best be made by comparing one of the lower curves in Figure 2.

Figure 1(d) corresponds to the light curve minimum. From this map it is clear that the dissipation at the stream-disc impact is at a minimum. This is because the spiral compression arm in the outer disc has moved such that gas is escaping from the primary Roche lobe and returning to the secondary. The gas leaving the L_1 point from the secondary encounters the disc gas instantly and the two flows have a low relative velocity. Hence relatively little dissipation is generated by the converging flows. At this phase the dissipation is dominated by the shear flow in the inner regions of the disc.

As the binary orbit proceeds, a large void opens up between the L_1 point and the accretion disc, as shown in Figure 1 (b) and (e) and the spiral arm which previously extended towards the L_1 region becomes detached from the disc under centrifugal forces and then falls back towards the disc. When this gas hits the disc, the impact causes a sudden rise in dissipation, corresponding to the spiky peak in the light curve at orbital phase ~ 0.36 , and to the upper inhomogeneous arc on Figure 1(e). Once this gas has been re-assimilated into the disc flow the dissipation falls again. The secondary continues its orbit around the disc, and the stream flow and the disc flow at the stream-disc impact point become increasingly misaligned. As the relative velocity of the two flows increases, the dissipation in the brightspot region correspondingly increases, until it reaches a maximum at orbital phase ~ 0.64 , shown in Figure 1 (c) and (f). As the orbit proceeds, the angle between the stream and disc flows at the impact point decreases again, until the next minimum is reached at orbital phase 1.022. Similar behaviour is seen in the simple 3D model, and was fully explored in RHP2001. We have

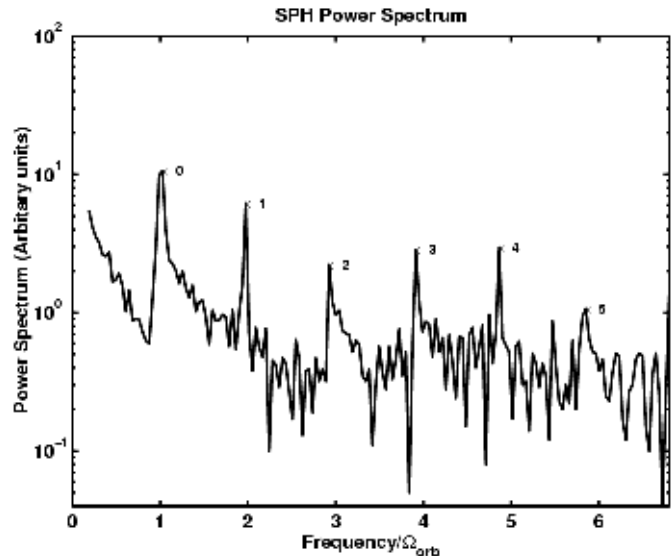


Figure 3. Power spectrum of the SPH dissipation light curve Figure 2 (a). The time series covered approximately 60 superhump periods with a resolution of $0.01\Omega_{orb}^{-1}$. The peak labelled 0 is the superhump frequency, the superhump harmonics are also labelled (1-5). The lower peaks correspond to linear combinations of Ω_{orb} , ω and Ω .

placed Microsoft AVI movies showing the surface dissipation in the SPH simulation and in the analytical model on the Internet site <http://physics.open.ac.uk/FHMR/>.

To determine the superhump period, P_{sh} , we took a Fourier transform of approximately sixty superhump cycles of the simulated light curve. The power spectrum is shown in Figure 3. The spectrum is plotted using a logarithmic scale to reveal the lower level peaks. A large peak that corresponds to the superhump period, labelled 0 in the figure, dominates the spectrum; the superhump harmonics have also been labelled (1-5). Using the power spectrum we estimated the superhump period to be $(1 + 0.0222 \pm 0.0005)P_{orb}$; this implies $P_{prec} = (46 \pm 1)P_{orb}$. The superhump period manifest in our simulation is in agreement with the analysis of Mineshige, Hirose & Osaki (1992). The other much lower amplitude periodicities present occur at frequencies Ω related to Ω_{orb} and disc apsidal precession frequency ω by:

$$k(\Omega - \omega) = j(\Omega - \Omega_{orb})$$

where k, j are positive integers.

3.3 Trailed Spectra

Kinematics in observed systems are revealed primarily by the spectral line profiles. To compare the results of the two simulations with CV and SXT observations we therefore generated synthetic emission line profiles and used these to build up synthetic trailed spectrograms.

An accretion disc emission line is Doppler broadened. Horne & Marsh (1986) calculated spectral line profiles from discs with smooth azimuthally symmetric line emissivity distributions, and Horne (1995) further included the effects of anisotropic turbulence on the local line broadening profile. We generated artificial emission line spectra for emissivity

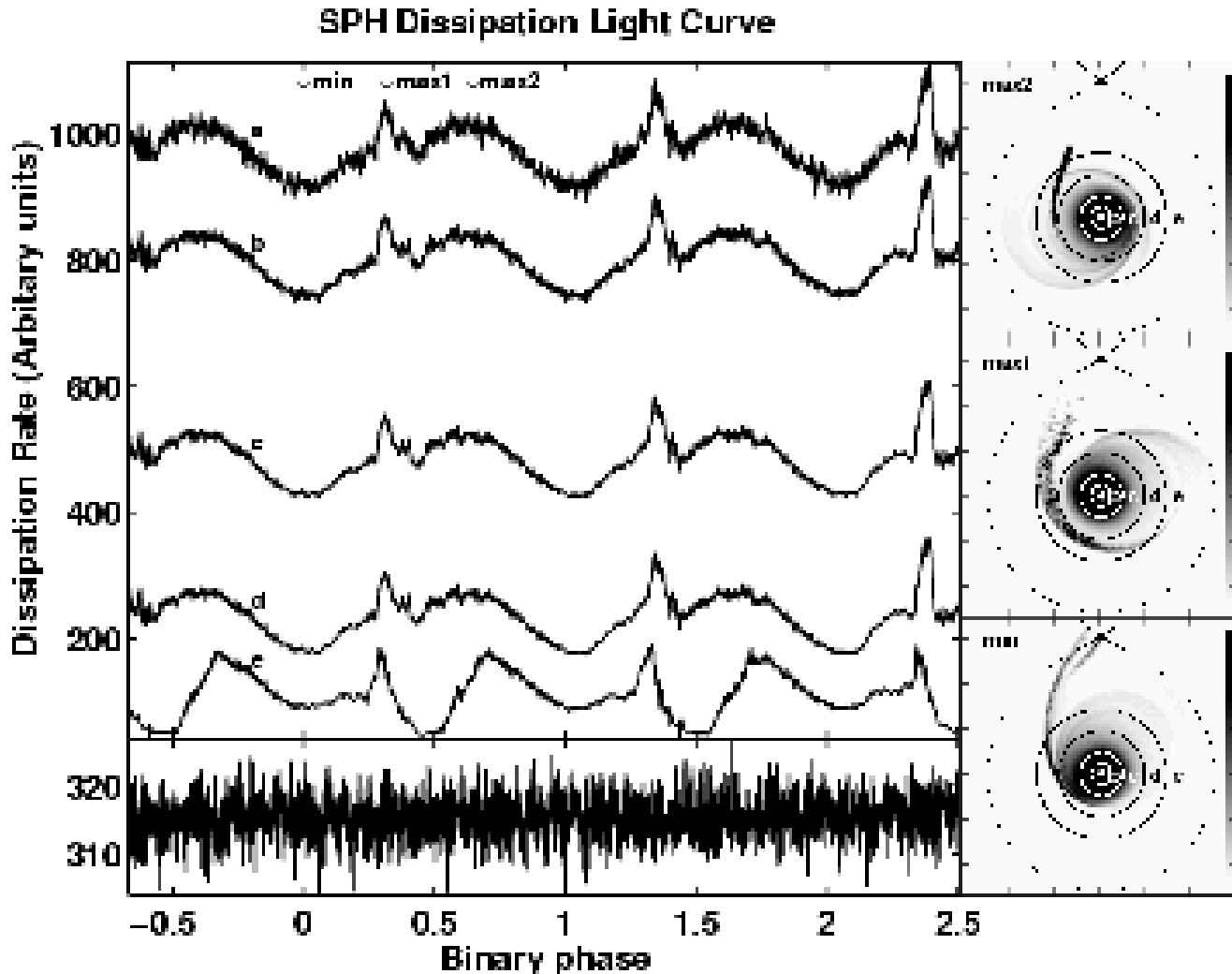


Figure 2. The top left plot is SPH viscous dissipation light curves for different regions of the accretion disc. The top curve, labelled *a*, is for the whole accretion disc, then each curve in descending order corresponds to dissipation from the disc at radii $> 0.05a$ (*b*), $> 0.1a$ (*c*), $> 0.2a$ (*d*) and $> 0.3a$ (*e*) respectively. The light curve minimum and two maximum points are indicated. The lower left-hand plot is the signal from the disc inner region and was generated by subtracting light curve *b* from light curve *a*. The plots on the right-hand side are disc dissipation maps that correspond to the light curve minimum and two maxima. The circles labelled *b*, *c*, *d* and *e* show the distances from the primary that correspond to the light curves *b*, *c*, *d*, *e* respectively.

distributions calculated from both the simple 3D code and the 2D SPH code.

For the simple 3D model we adopted Gaussian local line profiles with widths proportional to the disc thermal velocity; the brightspot emission was assumed to be thermally broadened using a brightspot temperature of 10^4K . We did not check for occultation of the accretion disc by the brightspot, but the 70° inclination was chosen to avoid eclipses by the secondary. Figure 4 shows three dissipation maps from the analytical model for orbital phases 0.00, 0.36 and 0.64 which correspond to the same orbital phases used in Figure 1. These maps show the dissipation plotted using a logarithmic greyscale with white low dissipation and black high. The primary Roche lobe has been plotted using a solid curve. The arrows indicate a fixed direction, as in Figure 1. The extent of the hotspot region is clearly visible in these maps. The simulated trailed spectra for two orbital periods

is shown in Figure 5 and the trailed spectra for a full disc precession cycle is shown in Figure 6.

Using the SPH model the dissipation from the accretion disc is divided into radial velocity bins. The emission in each velocity bin is the sum of the viscous dissipation from each particle within the velocity bin. For each SPH time step, $0.01\Omega_{orb}^{-1}$, an emission line profile was generated and shown in the trailed spectrogram in Figure 7. We have used a linear greyscale to represent dissipation intensity. The bottom of the spectrogram corresponds to the minimum flux point on the artificial light curve of Figure 2 (labelled ‘*min*’). At approximately orbital phase 0.36 (‘*max1*’) there is a large emission associated with the first large spiky hump on the light curve. At about orbital phase 0.64 (‘*max2*’) there are two distinctive emission arcs. These arcs are generated by the particles in the brightspot region. The lower arc is from the particles in the gas stream that collide with the parti-

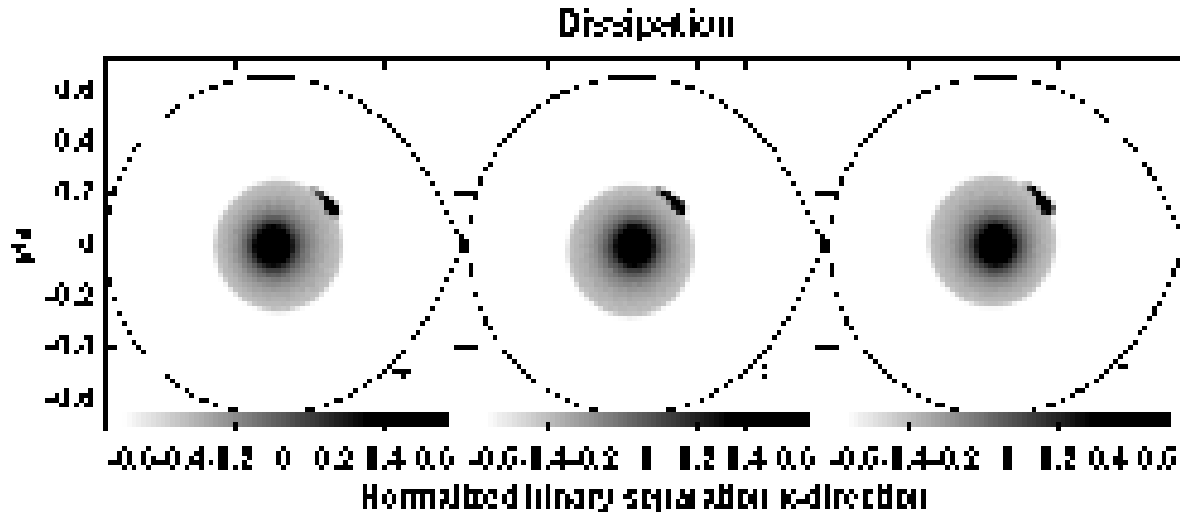


Figure 4. Dissipation maps for the accretion disc used in the analytical model. The dissipation is displayed using a logarithmic greyscale for binary phases 0.00, 0.36, and 0.64 respectively. The solid curve is the Roche lobe of the primary. The secondary’s orbital motion is vertically upwards. The arrow displayed in each map indicates a fixed direction to an observer, with phases defined as in Figure 1.

cles in the accretion disc. The other arc is the emission from the particles in the accretion disc that are in the brightspot region. The disc spiral density compression waves produce enhanced emission that can be seen in Figure 7 as features in the trailed spectrogram along the velocity lines $\sim 300 \text{ km s}^{-1}$ and $\sim -700 \text{ km s}^{-1}$. Figure 8 shows the trailed spectrogram for a complete disc precession cycle, equivalent to that of the simple 3D model in Figure 6.

All of our simulated trailed spectrograms are dominated by strong double-peaked emission which exhibits significant variability. Emission from the brightspot region is prominent in all spectrograms. In Figures 5 to 8 the summation of the emission horizontally and vertically is shown, so the upper panel is the mean line profile, and the right-hand panel is the light curve. The light curve in Figure 6 clearly shows the modulation in the superhump profile which was fully explored in RHP2001 and Rolfe (2001).

Figure 9 is a montage of SPH trailed spectra for different orbits sampling a complete disc precession. Each spectrogram uses the same linear greyscale and the number in the upper left-hand corner of each image indicates the disc precession phase. This figure clearly demonstrates the variability of accretion disc spectra with respect to disc precession phase. We have placed on the Internet a Microsoft AVI movie showing the spectrogram’s evolution over a complete disc precession cycle (<http://physics.open.ac.uk/FHMR/>). In order to compare our high resolution trailed spectra with current observations, we reduced the spectral and time resolution of each spectrogram of Figure 9 by a factor of 25 and the result is displayed in Figure 10.

In all of our trailed spectrograms we see the effects of the precessing disc. In Figure 6 we see a long period S-wave in the envelope of the disc emission, caused by the disc’s precession on P_{prec} . The orbital modulation in the brightspot emission causes the shorter timescale S-wave which is most clearly apparent where it crosses each of the two peaks in the line profile.

In Figure 7 we show the more complex orbital modula-

tion in the line profile which occurs in the SPH simulation. At first glance the pattern appears to repeat from orbit to orbit, but in fact there is a gradual evolution which can be clearly seen in Figures 8 and 9. The spectral pattern repeats after a complete disc precession period.

3.4 Doppler tomography

Doppler tomography was developed to interpret trailed spectrograms of CVs (Horne & Marsh 1988; Marsh 2000). Generally observers use a maximum-entropy inversion process to generate the most likely Doppler map from the spectra. Doppler tomography condenses the information in a trailed spectrogram into a velocity map of the emission regions in a system. The observed spectral line profiles as a function of orbital phase are inverted to reveal the best-fitting Doppler map of the line flux as a function of velocity in the binary frame. It implicitly assumes:

- the emission regions are fixed within the co-rotating frame
- the emission does not vary with time over the course of a binary orbit
- all points are visible at all times
- all motion is in the orbital plane
- the width of the profiles from any point is small

Our simulations, those described in (Murray 2000) and eclipse mapping of V348 Pup (Rolfe et al. 2000) reveal discs which violate the first two of these assumptions. Hence, for precessing non-axisymmetric discs, it is safer to work with trailed spectrograms directly rather than constructing Doppler tomograms. Nevertheless, many of the relevant observational publications in the last decade have included tomography, so we have constructed tomograms from our simulated line profiles.

Doppler maps represent the binary configuration in two-dimensional velocity-space. Figure 11 shows an example of an instantaneous Doppler map generated from the

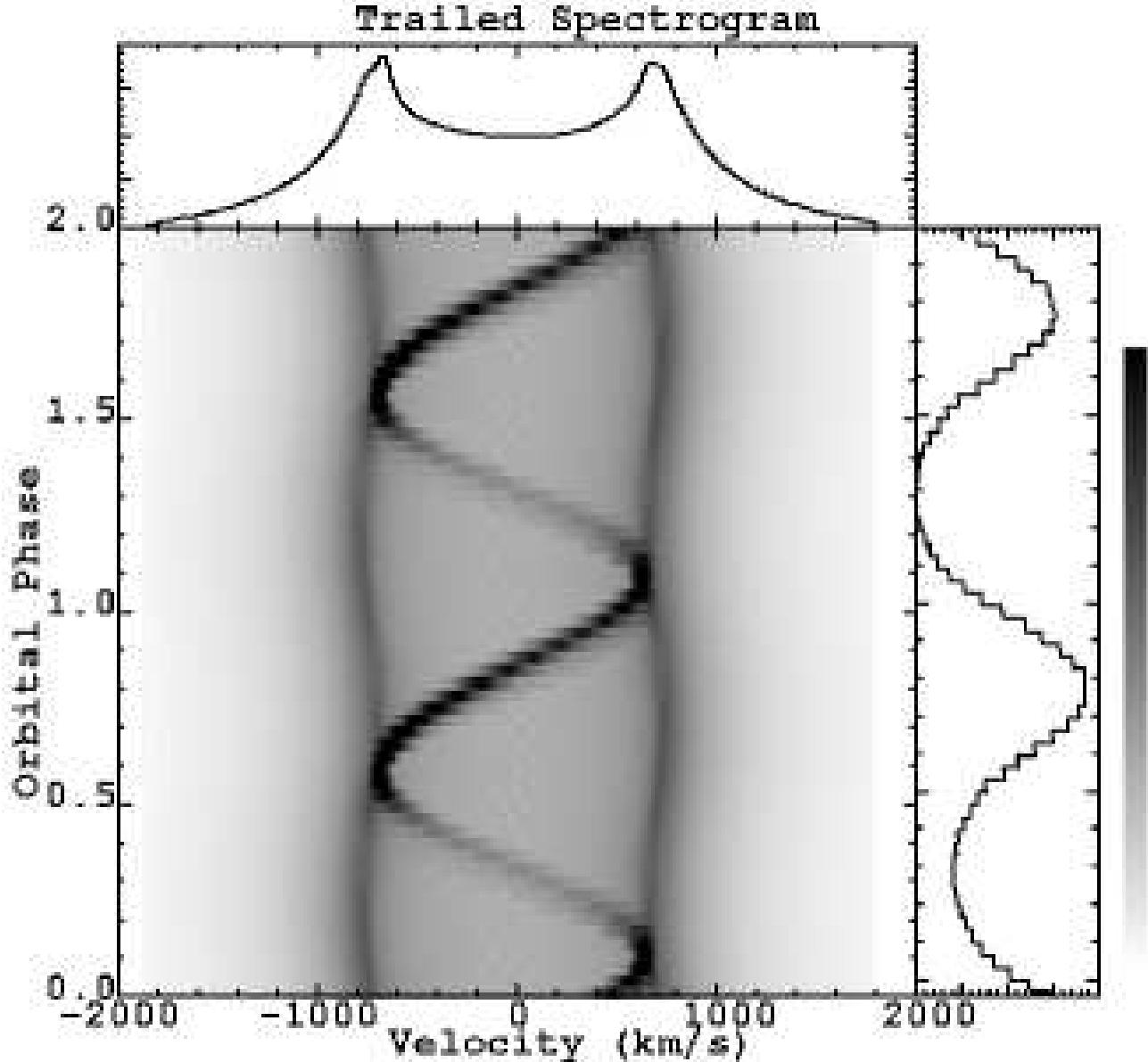


Figure 5. Trailed spectrogram using a linear greyscale for the analytical accretion disc model. The spectrogram is for two orbital periods. The curves on the top and right of the spectrogram are the average line flux vertically and horizontally respectively, i.e. they constitute a mean line profile and a light curve respectively.

SPH dissipation data. The primary and secondary velocities are overlaid on the Doppler map y-axis with the secondary having a positive y-velocity. The lower of the two overplotted arcs indicates the ballistic trajectory of the gas stream; the upper arc indicates the velocity of a circular Keplerian disc at positions along the ballistic stream trajectory: the stream’s ‘Kepler shadow’. The velocity of each particle is used to transform each particle into velocity space. The velocity density at each velocity cell in the Doppler map is the sum of the dissipation from each particle mapped to that cell, i.e. the number of particles occupying each velocity

cell multiplied by the particle dissipation, is plotted using a linear grey intensity scale.

Figure 1(*d, e, f*) demonstrates that the emission from the disc changes substantially in the course of a binary orbit, and is far from fixed in the co-rotating frame. Hence the instantaneous Doppler map varies significantly with orbital phase. Figure 1(*g, h, i*) shows detail of instantaneous Doppler maps corresponding to the dissipation snapshots in Figure 1(*d, e, f*).

The prominent dissipation near the letter “G” on Figure 1(*i*) arises from the gas stream as it impacts the outer edge of the accretion disc. This gas is accelerated until it has

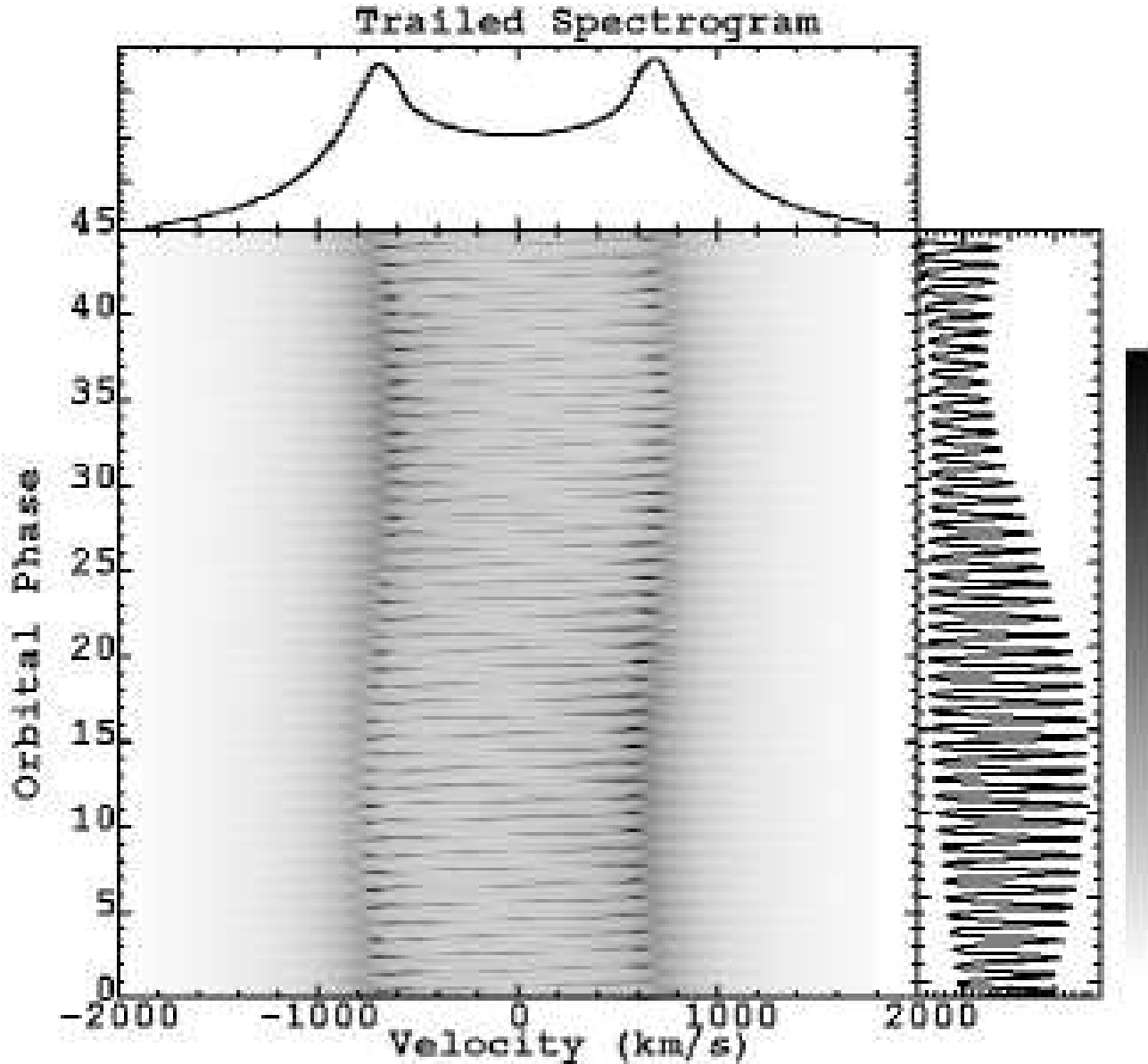


Figure 6. Trailed spectrogram using a linear greyscale for the simple 3D accretion disc model. The spectrogram is for a complete disc precession. The curves on the top and right of the spectrogram are the average flux vertically and horizontally respectively.

the same speed as the gas in the disc, producing the small very bright arc close to the impact point. The letter “H” on this Doppler map indicates the arc of emission produced by the disc particles in the impact region. As the two flows converge (progressing to velocity locations which move in an anti-clockwise sense) the relative velocity of the two arcs decreases to zero. Emission from the gas downstream of the impact point can be seen trailing away (anti-clockwise) from the brightspot impact point. The outer disc in the simulation does **not** consist of particles executing circular Keplerian orbits, so the disc velocity at the impact point does **not** generally lie on the Kepler shadow trajectory overplotted on the map.

In Figure 1(*g*) there are *three* arcs of enhanced emission. Two of them are produced by the stream particles and the disc particles at the impact; the third, uppermost, velocity arc is produced by emission from the centrifugally expelled material, which can be seen extending outside the primary Roche lobe in Figure 1(*d*). The material outside the lobe is moving up and slowly to the right in Figure 1(*d*), and so it appears in the upper right quadrant of the velocity map in Figure 1(*g*), where it extends across the donor velocity lobe.

The disc in our simulation is eccentric, precessing rapidly with respect to the co-rotating frame (since it is precessing only slowly in the inertial frame), and continuously flexing and relaxing on the superhump period. This causes

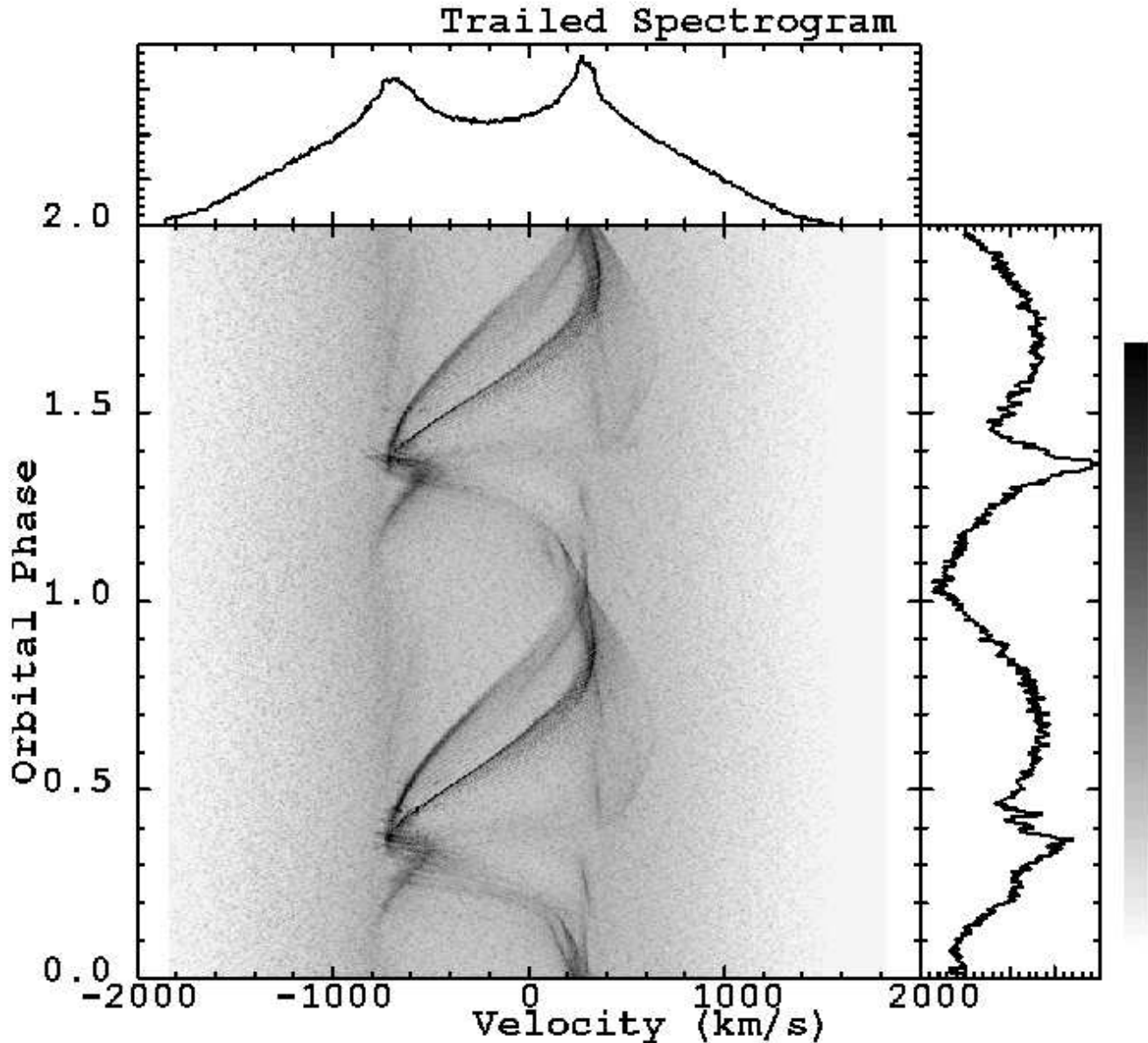


Figure 7. Trailed spectrogram using a linear greyscale for the SPH accretion disc model. See Figure 5 caption.

the appreciable changes in the instantaneous Doppler maps produced at different orbital phases, Figure 1(*g*, *h* and *i*).

Since observers cannot produce an instantaneous Doppler map, we show in Figure 12, middle image, a Doppler dissipation map for a complete orbital period. This map was generated by averaging the instantaneous Doppler maps for each model time step, $0.01\Omega_{orb}^{-1}$, i.e. 629 ($\approx 100 \times 2\pi$) instantaneous maps corresponding to a complete orbit were averaged. Two large emission arcs dominate this map. The lower arc is situated just above the gas stream ballistic trajectory and was generated by the gas stream impacting the outer edge of the accretion disc. The merging streams generate a large dissipation. The upper arc is generated by the particles in the accretion disc that interact with the gas stream

particles. These two bright arcs show the change of velocity (and position) of the impact region as a function of orbital phase. There is also another lower intensity arc in the lower left-hand quadrant. The source of this arc is one of the spiral density waves seen in Figure 1(*d*).

The SPH trailed spectrogram, shown in Figure 12, was inverted using DOPPLER, a maximum entropy Doppler tomography package developed by Tom Marsh⁴, and is shown in the bottom image of Figure 12. A constant Doppler map was generated using MAKIMG and then scaled using OPTSCL. The Doppler map had a starting chi-squared value of 26.6

⁴ <http://www.astro.soton.ac.uk/~trm/tar/doppler.tar.gz>

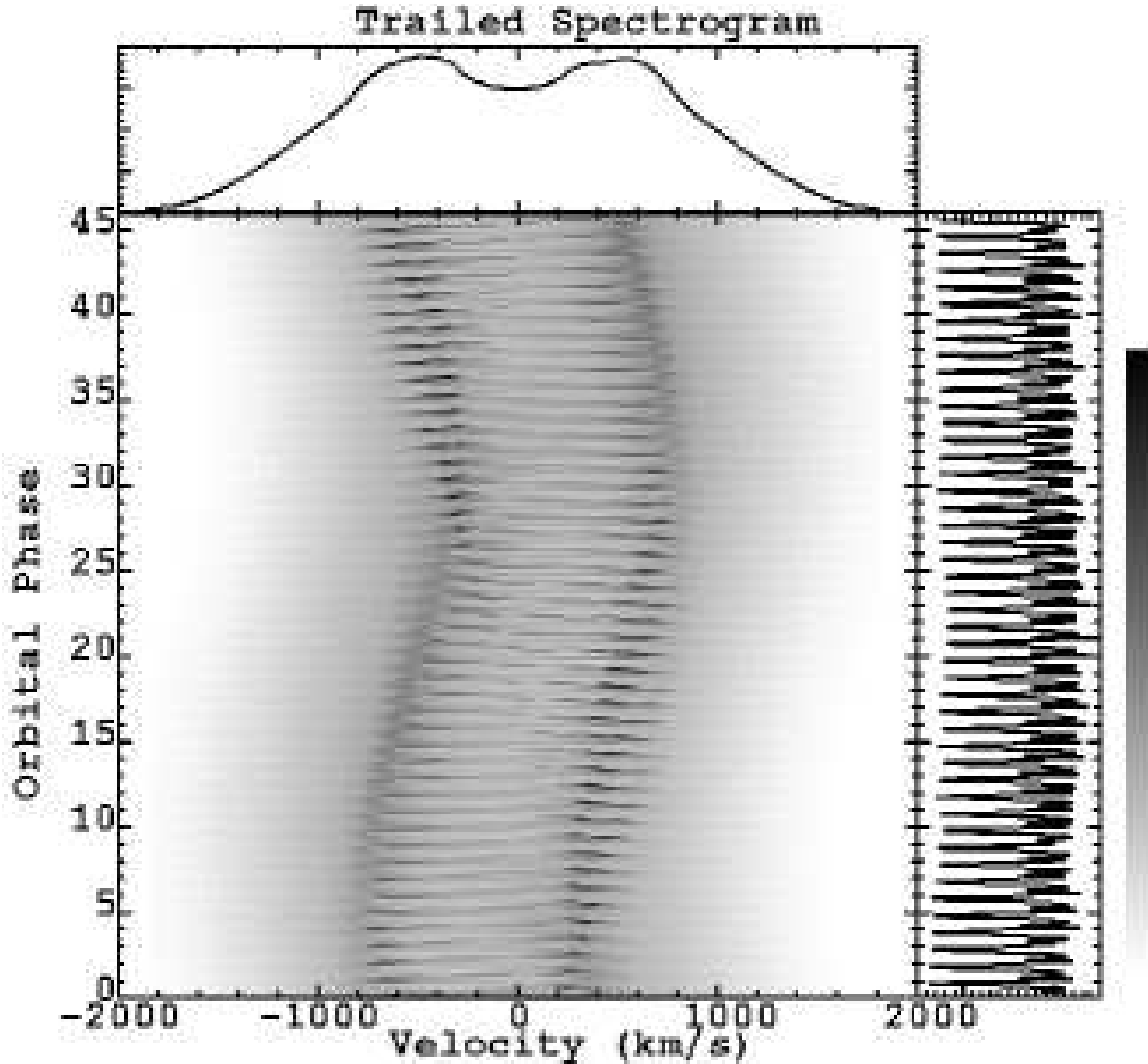


Figure 8. Trailed spectrogram using a linear greyscale for the SPH accretion disc model. The spectrogram is for a complete disc precession. The curves on the top and right of the spectrogram are the average flux vertically and horizontally respectively.

and was slowly reduced to 10.0 using MEMIT. The resulting maximum entropy Doppler map has a much reduced resolution compared to the Doppler map generated directly from the SPH simulation particle data (shown in the middle image of Figure 12) and the disc spiral density waves are now poorly defined. The inversion process has reproduced two high intensity emission arcs located near the gas stream ballistic path and the gas stream Kepler shadow, but their appearance differs from those in the direct SPH map. A number of artifacts are apparent in the maximum entropy map.

Figure 13 shows a Doppler map using the velocity data from the 3D analytical model over a full orbital period.

The Doppler map was generated using the filtered back-projection routine in the MOLLY⁵ spectral analysis software. This Doppler map is dominated by a large emission arc associated with the dissipation from the hotspot region. The location of this emission arc lies between the gas stream ballistic path and the gas stream Kepler shadow.

Our SPH tomograms, Figures 1, 11 and 12, show that the emission from the stream-disc impact can appear outside the region between the ballistic stream trajectory and its Kepler shadow. In particular, the strongest emission from

⁵ <http://www.warwick.ac.uk/staff/T.R.Marsh/molly.tar.gz>

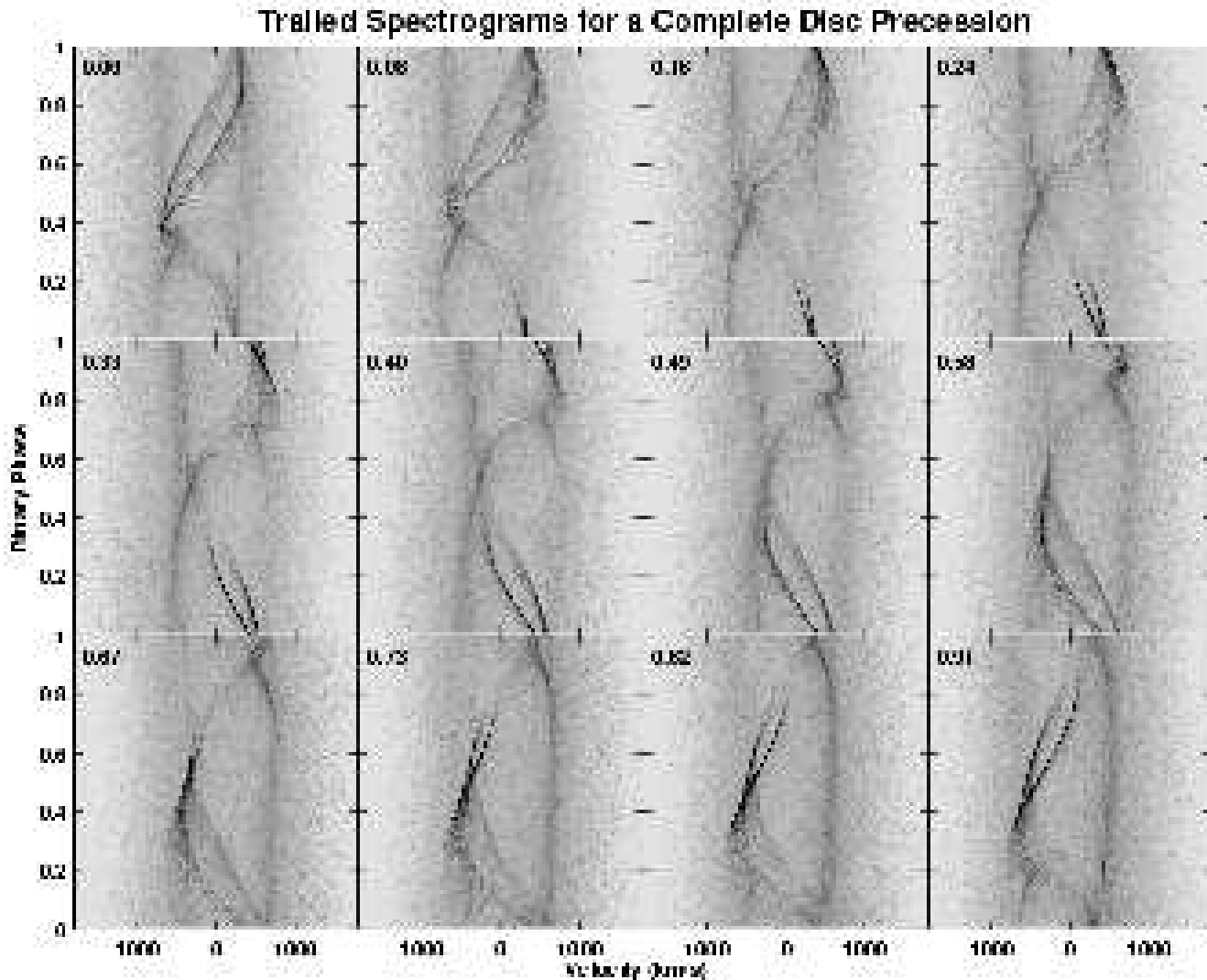


Figure 9. Trailed spectrograms for a complete disc precession from the SPH simulation. The spectrograms use a linear greyscale and the number in the upper left-hand corner of each image indicates the disc precession phase.

the impact (‘H’ in Figure 1(i)) is outside this region. Hence tomographic analysis such as the determination of K_2 for AM CVn by Nelemans, Steeghs & Groot (2001) may be flawed.

4 DISCUSSION & CONCLUSIONS

We have presented two simulations of a binary system with an extreme mass ratio of $q = 0.1$. Using a SPH simulation of the accretion disc we find the disc to be eccentric, non-axisymmetric and precessing in the inertial frame.

The light curve in our SPH simulation shows complex variations with a short duration spiky peak superimposed on a smoother modulation. The light curve roughly repeats on the superhump period, but evolves continuously from cycle to cycle, as the example of two consecutive orbits shown in Figure 7 shows. The power spectrum of the simulated light curve is dominated by the superhump frequency and its harmonics.

Simulated SPH trailed spectrograms show complex fine structure that changes from one orbit to the next. A full disc precession cycle elapses before the trailed spectrogram repeats. The trailed spectra have changing features that include two very bright emission arcs associated with the impact of the gas from the donor star on the outer edge of the accretion disc. The 3D model trailed spectrograms show less complexity than the SPH model. These spectrograms show bright ‘S’ wave features that slowly change as the elliptical disc precesses in the binary frame. The simulated dissipation light curve from this model is also modulated due to the precession of the accretion disc.

The differences in the trailed spectrograms arise from the differences in the two models: the 3D model underlying Figure 6 smoothly distributes weight across all the mass in the disc. Its precursor was generated to explain the skewed absorption lines produced by AM CVn’s precessing disc (Patterson et al. 1993b). In contrast, the SPH trailed spectrogram (Figure 8) is weighted by dissipation. Consequently it reveals those locations where the flow is strongly sheared,

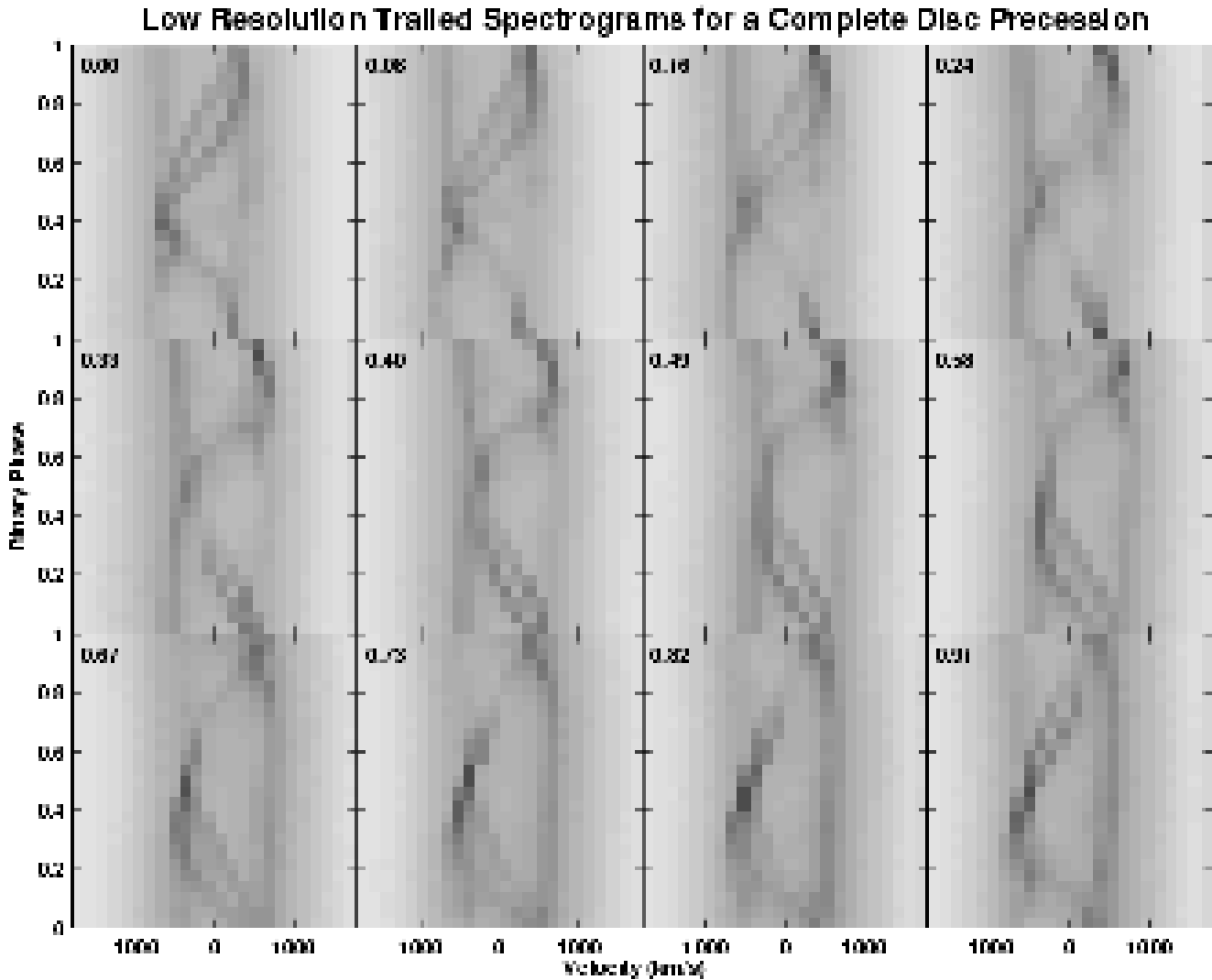


Figure 10. Low-resolution trailed spectrograms for a complete disc precession from the SPH simulation. The spectrograms use a linear greyscale and the number in the upper left-hand corner of each image indicates the disc precession phase.

or subject to compression under the tidally-modulated flexing. These regions will contribute disproportionately to emission line production. Hence, treating the disc component as in section 2.2 may be more appropriate for comparison with absorption lines from precessing discs, while the approach of section 2.3 is more appropriate for comparison with emission lines produced by such discs.

Only 8 CVs and 8 LMXBs of ~ 600 systems listed in Ritter and Kolb (2003) have measured mass ratios $q \leq 0.125$. To our knowledge none of these have been observed extensively enough to produce trailed spectrograms uniformly sampling the disc precession cycle. The best observations to compare with our simulations are those of XTE J1118+480 in its 2000 outburst. Torres et al. (2002) show trailed spectrograms taken at four epochs during the outburst, from which they generate Doppler tomograms. At all epochs these tomograms are dominated by emission from the stream-disc impact region. The spectrograms are of considerably lower signal-to-noise ratio than those shown in Figure 10 but it is clear that the brightest emission moves from the red side (at

orbital phase ~ 1 ; c.f. disc precession phase 0.24 in our SPH trails) to the blue side (at orbital phase ~ 0.5 ; c.f. disc precession phase 0.73 in our SPH trails) over an interval of ~ 20 days. It is clear that the observed S-wave is non-sinusoidal, and its shape changes. These characteristics are all seen in our simulations. Further, higher resolution, observations of XTE J1118+480 (Haswell et al 2004) show in more detail that the observed S-waves exhibit shapes and phasing consistent with our simulations. VW Hyi, a CV with $q \approx 0.17$ (Schoembs & Vogt 1981), shows hints of two distinct S-waves in the trailed spectrogram presented in Figure A.14 of Tapert et al (2003), though the signal-to-noise ratio is again rather lower than in our simulated trails. We conclude our SPH simulations do appear to reproduce at least some observed characteristics of some extreme mass ratio systems.

Instantaneous Doppler maps generated from the SPH simulation show bright arcs created by the impact of the gas stream with the outer edge of the accretion disc. As the gas stream interacts with the disc material much energy is dissipated. Integration of the SPH instantaneous Doppler maps

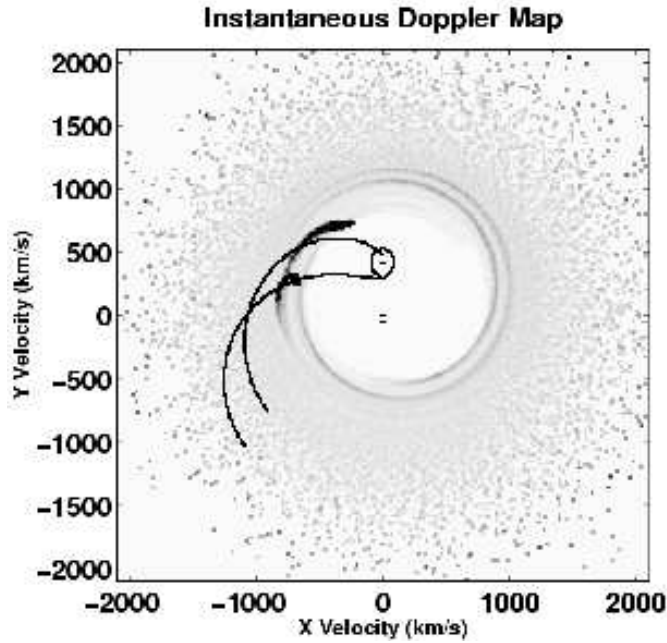


Figure 11. An instantaneous SPH model Doppler map. The top small black cross is the velocity co-ordinate of the secondary. The other two small black crosses are the velocity co-ordinates of the centre of mass of the binary system and the primary respectively. The predicted velocities of the gas stream are plotted and the velocities of the accretion along the gas stream. The velocity projection of the secondary's Roche lobe is also plotted.

over a full binary orbit shows two large very bright emission arcs resulting from the changing shape of the accretion over a binary period. The arcs indicate the changing velocities at the impact point. The 3D model Doppler map shows a single large emission arc associated with the brightspot region and is located between the gas stream and the stream's 'Kepler shadow', see Figure 13.

In our simulations, the stream-disc impact region is a prominent source of dissipation. It is generally accepted that for CVs in superoutburst tidally-modulated viscous dissipation in the bulk of the disc generates the superhump light (e.g. Murray 2000). These are known as normal or 'early' superhumps. These sometimes evolve to 'late' superhumps as the disc returns to its low-viscosity quiescent state. In late superhumps the stream-disc impact dissipation is a prominent feature of the CV light curve (RHP2001). As we noted in section 2.3, the prominence of the stream-disc impact region may to some extent be an artifact of our 2D simulations. However this region was also observed to be prominent in the outburst trailed spectra of XTE J1118+480. As XTE J1118+480 returned to quiescence, Zurita et al. (2002) observed trailed spectra in which the S-wave is much less prominent. This observed behaviour is exactly the opposite of the accepted picture for CVs. We can think of (at least) two possible reasons for this: (i) It is possible that the fraction of the total dissipation which occurs at the stream disc impact region is a function of mass ratio, becoming dominant in outburst for very extreme mass ratio systems like that simulated herein. (ii) The line emission in SXTs is likely to be powered by photo-ionisation. Thus, the observed prominence of the stream-disc impact may simply indicate

Trailed Spectrum and Doppler Maps

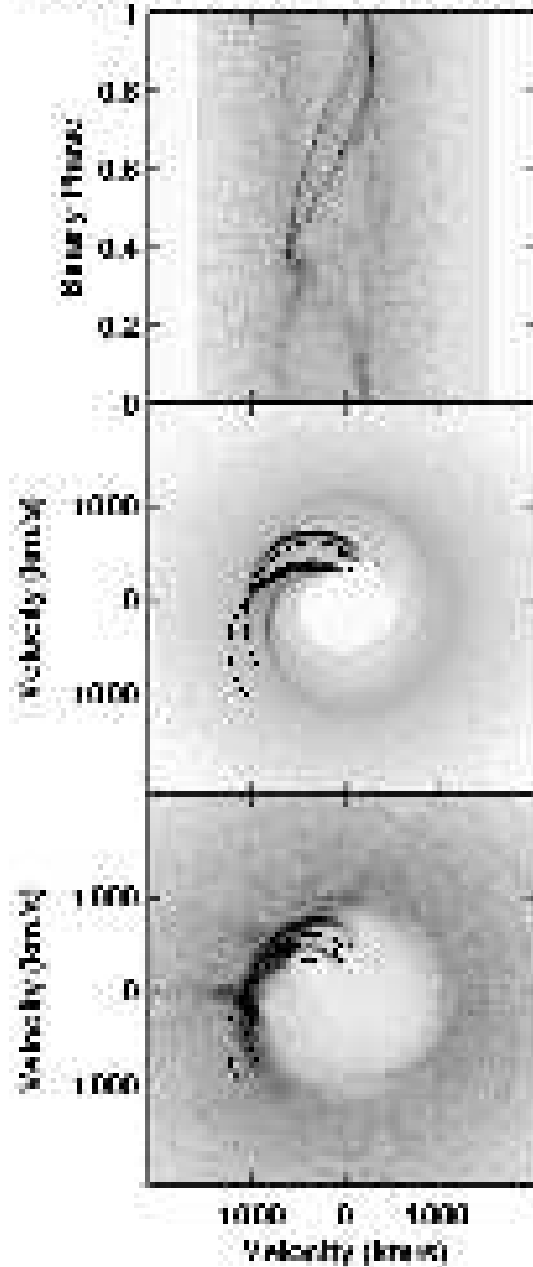


Figure 12. The top image is a SPH simulation trailed spectrogram for a single orbit. The middle image is the corresponding direct SPH model Doppler map, which was calculated by summing the instantaneous Doppler maps for each timestep in the orbit. The high intensity emission arc near the stream ballistic path was generated by the particles in the gas stream colliding with the outer edge of the accretion disc. The upper bright arc was generated by the disc particles in the impact region. The bottom image is the corresponding maximum entropy Doppler tomogram.

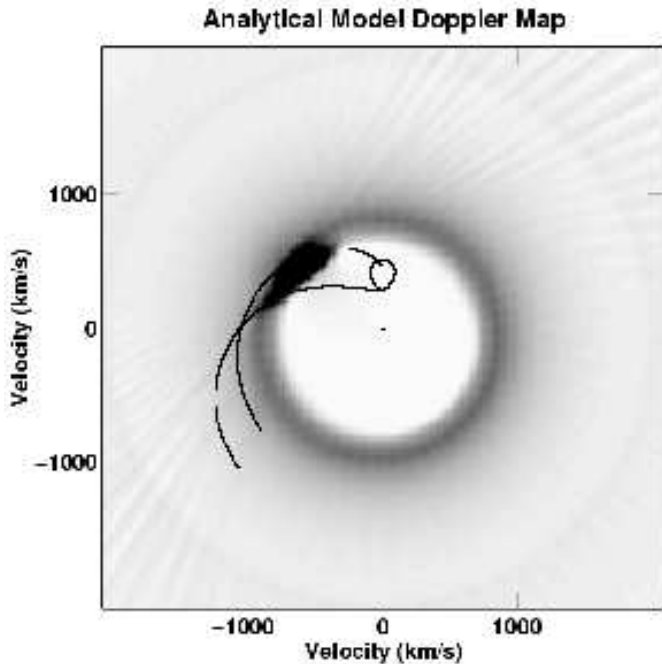


Figure 13. Analytical model Doppler map. See caption of Figure 11

that this region is raised above the surface of the bulk of the disc, and subtends a relatively large solid angle to the central X-ray source.

Once started, disc precession tends to persist (Murray 2000). Hence attempts to study SXTs upon their return to quiescence are likely to be complicated by phenomena related to disc precession (Haswell 1996). For example, Figure 8 shows that there is a radial velocity modulation on the disc precession period. The blue peak of the line profile moves from $\sim 400 \text{ km s}^{-1}$ at around orbital phase = 30 to $\sim 800 \text{ km s}^{-1}$ at around orbital phase = 10. An analogous, but smaller modulation is seen in Figure 6. A small part of this difference is because the SPH trailed spectrogram corresponds to an orbital inclination of 90° while the simple 3D model uses $i = 70^\circ$; the SPH velocities would be reduced by a factor 0.94 if $i = 70^\circ$. The main reason for the larger velocity modulation in the SPH simulation is the velocities of the strong dissipation at the stream-disc impact region vary much more than those in the simple analytic model.

Attempts have been made to measure the orbital motion of accreting compact objects by studying the emission lines from their accretion discs (Haswell & Shafter 1990; Orosz et al. 1994; Soria et al. 1998). Generally these observations are made over several nights, sampling parts of a number of orbits, interrupted by daylight intervals. The line profile measurements are then generally binned or folded on orbital phase and the ‘orbital’ motion measured by fitting a sine wave to the radial velocities. Figures 6 - 10 demonstrate that for a precessing disc this procedure is flawed because the line profiles do not repeat from orbit to orbit. Figure 8 shows that the radial velocity of the outer wings of the disc emission line is as strongly modulated on disc precession phase as it is on orbital phase. Random, non-uniform sampling of disc precession phase explains why Haswell & Shafter (1990) and Orosz et al. (1994) found emission line radial velocity

curves which were not in phase with the compact object’s orbital motion (as inferred from the mass donor star’s motion). In contrast, for binaries where the mass ratio is not extreme enough for the disc to extend out to the 3:1 resonance ($q \gtrsim 0.3$) the disc is not expected to be eccentric and precessing. For such systems it may be possible to measure the orbital radial velocity of the compact object, if contamination of the result by the brightspot and any other non-axisymmetric features is avoided. Indeed, for GRO J1655-40 which has a mass ratio of $q = 0.42$ (Shahbaz 2003), Soria et al. (1998) found an emission line radial velocity curve which *is* phased as expected for the orbital motion of the black hole. In CVs, the smaller dynamic range between the inner and outer disc radii may make measurements uncontaminated by the brightspot more challenging, nonetheless Unda-Sanzana et al. are finding encouraging results for U Gem which has $q > 0.3$ (Unda-Sanzana & Morales-Rueda, private communication).

5 ACKNOWLEDGEMENTS

SBF acknowledges the support from QinetiQ, Malvern, in particular from David Hutber. SBF and DJR would like to thank Tom Marsh for the use of his MOLLY and DOPPLER software. CAH acknowledges support from the Leverhulme Trust F/00-180/A during the early stages of this work. DJR was supported by a PPARC studentship and a PPARC PDRA. Theoretical astrophysics research at Leicester is supported by a PPARC rolling grant. SBF, CAH and JRM acknowledge support from the Open University’s Research School. We would also like to thank an anonymous referee for a very detailed report and for the many useful suggestions.

REFERENCES

- Armitage P., Livio M., 1996, *ApJ*, 457, 332
- Armitage P., Livio M., 1998, *ApJ*, 493, 898
- Haswell C. A., Shafter A. W., 1990, *ApJ*, 359, L47
- Haswell C. A. 1996, *IAU Symposium* 165, 351
- Haswell C. A., King A. R., Murray J. R., Charles P. A., 2001, *MNRAS*, 321, 457, [ArXiv:astro-ph/0008367](https://arxiv.org/abs/astro-ph/0008367)
- Haswell C. A., Rolfe D. J., Tovmassian G., Maxted P., North R., Hynes R., 2004, in preparation
- Hessman F. V., Manter K. H., Barwig H., Schoembs R., 1992, *A&A*, 263, 147
- Hessman F. V., 1999, *ApJ*, 510, 867
- Horne K., Marsh T. R., 1986, *MNRAS*, 218, 761
- Horne K., Marsh T. R., 1988, *MNRAS*, 235, 269
- Horne K. 1995, *A&A*, 297, 273
- Kunze S., Speith R., Hessman F. V., 2001, *MNRAS*, 322, 499
- Lubow S. H., 1991, *ApJ*, 381, 259
- Marsh T. R., 2000, [arXiv:astro-ph/0011020](https://arxiv.org/abs/astro-ph/0011020)
- Mineshige S., Hirose M., Osaki Y., 1992, *PASJ*, 44, L15
- Monaghan J. J., 1992, *ARA&A*, 30, 543
- Murray J. R., 1996, *MNRAS*, 279, 402
- Murray J. R., 1998, *MNRAS*, 297, 323
- Murray J. R., 2000, *MNRAS*, 314, L1
- Nelemans G, Steeghs D., Groot P.J., 2001, *MNRAS*, 326, 621
- Orosz J.A., Bailyn C.D., Remillard R.A., McClintock J.E., Foltz C.B., 1994, *ApJ*, 436, 8480
- Osaki Y., 1985, *A&A*, 144, 369

- Patterson J., Thomas G., Skillman D.R., Diaz M., 1993a, *ApJS*, 86, 235
Patterson J., Halpern J., Shambrook A., 1993b, *ApJ*, 419, 803
Patterson J., 1998, *PASP*, 110, 1132
Ritter H., Kolb U. 2003, *A&A*, 404, 301
Rolfe D.J., Haswell C. A., Patterson J., 2000, *MNRAS*, 319, 467
Rolfe D.J., Haswell C. A., Patterson J., 2001, *MNRAS*, 324, 529
Rolfe D.J., 2001, Ph.D. thesis, The Open University.
Schoembs R., Vogt N. 1981, *A&A*, 97, 185.
Shahbaz T., 2003, *MNRAS*, 339, 1031
Shakura N. I., Sunyaev R. A., 1973, *A&A*, 24, 337
Soria R., Wickramasinghe D.T., Hunstead R.W., Wu K., 1998, *ApJ*, 495, L95
Tappert C., Mennickent R.E., Arenas J., Matsumoto K., Hanuschik R.W. 2003, *A&A*, 408, 651
Torres M. A. P., Callanan P. J., Garcia M. R., McClintock J. E., Garnavich P., Balog Z., Berlind W. R., Calkins M., Mahdavi A., 2002, *ApJ*, 569, 423, arXiv:astro-ph/0112462
Truss M. R., Murray J. R., Wynn G. A., Edgar R. G., 2000, *MNRAS*, 319, 467
Vogt N., 1982, *ApJ*, 252, 653
Zurita C., Casares J., Shahbaz T., Wagner R. M., Foltz C. B., Rodriguez-Gil P., Hynes R. I., Charles P. A., Ryan E., Schwarz G., Starrfield S. G., 2002, *MNRAS*, 333, 791